Eur. Phys. J. C 53, 267–280 (2008)
DOI 10.1140/epjc/s10052-007-0453-x

THE EUROPEAN PHYSICAL JOURNAL C

Regular Article – Theoretical Physics

Associated charged Higgs and W boson production in the MSSM at the CERN large hadron collider

D. Eriksson[1,a], S. Hesselbach[1,2], J. Rathsman[1]

[1] High Energy Physics, Uppsala University, Box 535, 75121 Uppsala, Sweden
[2] Institut für Theoretische Physik und Astrophysik, Universität Würzburg, 97074 Würzburg, Germany

Received: 18 December 2006 / Revised version: 28 September 2007 /
Published online: 16 November 2007 –

Abstract. We investigate the viability of observing charged Higgs bosons ($H^{\pm}$) produced in association with W bosons at the CERN large hadron collider, using the leptonic decay $H^+ \to \tau^+\nu_\tau$ and hadronic W decay, within different scenarios of the minimal supersymmetric standard model (MSSM) with both real and complex parameters. Performing a parton level study we show how the irreducible standard model background from $W+2$ jets can be controlled by applying appropriate cuts and find that the size of a possible signal depends on the cuts needed to suppress QCD backgrounds and misidentifications. In the standard maximal mixing scenario of the MSSM we find a viable signal for large $\tan\beta$ and intermediate $H^{\pm}$ masses ($\sim m_t$) when using softer cuts ($\not{p}_\perp, p_{\perp\tau_{\rm jet}} > 50\,\text{GeV}$), whereas for harder cuts ($\not{p}_\perp, p_{\perp\tau_{\rm jet}} > 100\,\text{GeV}$) we only find a viable signal for very large $\tan\beta$ ($\gtrsim 50$). We have also investigated a special class of MSSM scenarios with large mass splittings among the heavy Higgs bosons where the cross-section can be resonantly enhanced by factors up to one hundred, with a strong dependence on the CP-violating phases. Even so we find that the signal after cuts remains small except for small masses ($\lesssim m_t$) when using the softer cuts. Finally, in all the scenarios we have investigated we have only found small CP-asymmetries.

1 Introduction

The quest for understanding electroweak symmetry breaking and the generation of elementary particle masses is one of the driving forces behind the upcoming experiments at the CERN large hadron collider (LHC). In the standard model (SM) the electroweak symmetry is broken by introducing one Higgs doublet whereas in the minimal supersymmetric standard model (MSSM), which is the main focus of this paper, two Higgs doublets are needed. More specifically, the MSSM is a two Higgs doublet model (2HDM) of type II where one of the doublets gives mass to all the up-type fermions and the other to all the down-type fermions. After electroweak symmetry breaking the Higgs sector in the MSSM consists of three neutral Higgs bosons and one charged one. The charged Higgs boson ($H^{\pm}$) is of special interest, since there are no charged scalars in the SM and thus its discovery would constitute an indisputable proof of physics beyond the standard model. Therefore, the hunt for charged Higgs bosons will play a central role in the search for new physics at the LHC experiments.

Currently the best model-independent direct limit on the charged Higgs boson mass is from the LEP experiments, $m_{H^{\pm}} > 78.6\,\text{GeV}$ (95% CL) [1] (assuming only the decays $H^+ \to c\bar{s}$ and $H^+ \to \tau^+\nu_\tau$). In addition, there are stronger direct limits from the Fermilab Tevatron, but only for very large or very small $\tan\beta$ ($\tan\beta \gtrsim 100$ and $\tan\beta \lesssim 1$, respectively), where $\tan\beta$ denotes the ratio of the vacuum expectation values of the two Higgs doublets, as well as indirect limits mainly from B decays although the latter are quite model-dependent. We refer to the PDG [2] for details.

The main production mode of charged Higgs bosons at hadron colliders is in association with top quarks through the $gb \to H^-t$ and $gg \to H^-t\bar{b}$ processes [3–6] with the former one being dominant for heavy charged Higgs bosons $m_{H^{\pm}} \gtrsim m_t$ and the latter one for light ones $m_{H^{\pm}} \lesssim m_t - m_b$. The possibilities of detecting charged Higgs bosons in these channels have been studied extensively (see for example [7–13] and also more specifically for the two LHC experiments [14–16]). In summary, the leptonic decays $H^+ \to \tau^+\nu_\tau$ seem to be most promising for detecting light charged Higgs bosons at any value of $\tan\beta$ and heavy charged Higgs bosons for large $\tan\beta$ whereas the hadronic decays $H^+ \to t\bar{b}$ may be useful both for large and small $\tan\beta$ above threshold. However, the transition region $m_{H^{\pm}} \sim m_t$ has so far been difficult to cover and the same is true for the intermediate $\tan\beta \sim \sqrt{m_t/m_b}$ region, except in special supersymmetric scenarios with decays into charginos and neutralinos [17–19]. The possibility of using the $gg \to H^-t\bar{b}$ process to improve the discovery potential in the transition region has been studied in [20, 21]. Recently a new method for matching the differential cross-sections for the two production modes has

[a] e-mail: david.eriksson@tsl.uu.se

been developed [22], resulting in a significantly improved discovery potential in the transition region [23].

Given the problems with exploiting the production of charged Higgs bosons in association with top quarks it is also important to investigate other production modes. One primary example is the production in association with W bosons [24–33]. In addition to being a complement to the main production mode, especially in the transition region, this channel may also give additional information on the Higgs sector. So far, $H^\pm W^\mp$ production has mainly attracted theoretical interest with limited attention to the experimental viability, the only exception being [26] which came to the conclusion that in the MSSM the signature $W^\pm H^\mp \to W^\pm tb \to W^\pm W^\mp bb$ cannot be used due to the irreducible background from $t\bar{t}$ production. On the contrary, in this paper we will show that the situation may be drastically improved, at least for large $\tan\beta$, by instead looking at leptonic decays $H^+ \to \tau^+\nu_\tau$ together with $W \to 2$ jets. Alternatively, going to a more general 2HDM one can get a very large enhancement of the production cross-section compared to the MSSM through resonant enhancement [33]. The associated production of charged Higgs bosons with CP-odd scalars A and subsequent leptonic $H^+ \to \tau^+\nu_\tau$ decays have been analyzed in [34].

Different types of higher order corrections to $H^\pm W^\mp$ production that have been studied typically give effects of the order 10%–20%. This includes the supersymmetric electroweak corrections [30], the next-to-leading order (NLO) QCD corrections [31], and the supersymmetric QCD corrections [32]. Of special importance here are the NLO QCD corrections since they show that one has to use running masses for the Yukawa couplings, which in turn has a large impact on the magnitude of the cross-section as will be discussed later. In addition, to process specific higher order corrections there are also higher order effects from the bottom/sbottom sector in supersymmetric theories that are large for large $\tan\beta$ and therefore have to be resummed to all orders in perturbation theory [35, 36]. This results in additional terms proportional to Δm_b in an effective Lagrangian [36] describing the couplings of charged Higgs bosons to top and bottom quarks. Finally we expect that a variation of the SUSY scenario, especially of μ, will lead to a variation of the cross-section of $\mathcal{O}(10\%)$ [37]. Since we will only be studying the $H^\pm W^\mp$ production at parton level, although with appropriate smearing of momenta, we have chosen not to take into account any of these corrections in the production, except for the use of a running b-quark mass in the Yukawa coupling.

The study of $pp \to H^\pm W^\mp$ also offers the possibility to explore effects of CP-violation. In the MSSM with complex parameters one gets new sources of CP-violation beyond the CKM matrix which can give rise to explicit CP-violation also in the Higgs sector through loops of supersymmetric particles [38, 39]. For example, such phases may give rise to differences in the $\mu^+\mu^- \to W^+H^-$ and $\mu^+\mu^- \to W^-H^+$ cross-sections which have been analyzed in a more general CP-violating 2HDM [40] although not taking into account non-diagonal Higgs propagator effects [41, 42]. Another example is the CP-odd rate asymmetry induced by loops of SUSY particles in the decay $H^+ \to t\bar{b}$ [43] that has been analyzed for the LHC in [44].

The outline of this paper is as follows: we start by giving the differential cross-section for the dominant production mode of charged Higgs bosons in association with W bosons for large $\tan\beta$ and study the dependence on $m_{H^\pm}$ and $\tan\beta$ at the LHC. In Sect. 3, we then specialize to the decays $H^+ \to \tau^+\nu_\tau$ and $W^- \to 2$ jets, and we compare signal and background giving special attention to the difficult transition region where $m_{H^\pm} \sim m_t$ and the leptonic decay mode of the charged Higgs boson is dominant. We show how the irreducible SM background for the resulting signature $\tau\not{p}_\perp + 2$ jets can be substantially reduced by appropriate cuts. In Sect. 4, we then give the results of our study in the MSSM both with real and complex parameters. In the latter case we investigate the possible dependence of the signal on some of the CP-violating phases of the MSSM. We also study a class of special scenarios within the MSSM where the cross-section is resonantly enhanced. Finally, Sect. 5 contains our conclusions.

2 $H^\pm W^\mp$ production at the LHC

In this section we give the differential cross-section for the dominant production mode of charged Higgs bosons in association with W bosons at large $\tan\beta$ in a general type II 2HDM and then specialize to the case of the maximal mixing scenario in the MSSM giving the dependence of the total cross-section on $m_{H^\pm}$ and $\tan\beta$ at the LHC.

2.1 Differential cross-section

In a general 2HDM of type II, the dominant production mechanisms for a charged Higgs boson in association with a W boson at hadron colliders are $b\bar{b}$ annihilation,

$$b\bar{b} \to H^\pm W^\mp\,, \tag{1}$$

at tree-level and gluon fusion,

$$gg \to H^\pm W^\mp\,, \tag{2}$$

at one-loop level [24, 25]. In this study we focus on the parameter region with intermediate $H^\pm$ masses ($\sim m_t$) and large $\tan\beta$, where the decay $H^\pm \to \tau\nu_\tau$ has a large branching ratio and where the $b\bar{b}$ annihilation dominates, and thus we do not need to consider the contribution from gluon fusion. Note that this is true also in MSSM scenarios with large $\tan\beta$, light squarks and large mixing in the squark sector, because the possible strong enhancement of the gluon fusion cross-section through squark loops occurs only for small $\tan\beta \lesssim 6$–7 [29].

The Feynman diagrams for $b\bar{b} \to H^\pm W^\mp$ are shown in Fig. 1. The $b\bar{b}$ annihilation proceeds either via s-channel exchange of one of the three neutral Higgs bosons in the 2HDM or t-channel exchange of the top quark.

In the real 2HDM there are two CP-even, neutral Higgs bosons, h^0 and H^0, and one CP-odd one, A^0, whereas in

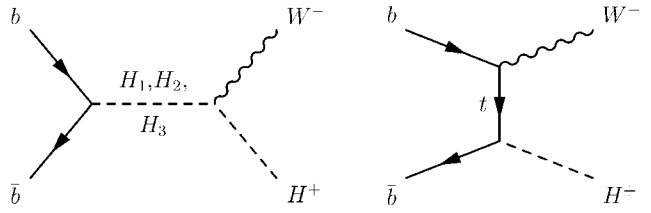

Fig. 1. Feynman diagrams for $H^\pm W^\mp$ production via $b\bar{b}$ annihilation, $b\bar{b} \to H^+W^-$

the general complex case all three neutral Higgs bosons mix and form three mass eigenstates H_i, $i = 1, \ldots, 3$. The Lagrangians relevant for the $b\bar{b} \to H^+W^-$ process are, following the conventions of [40, 45, 46],

$$\mathcal{L}_{H_i H^\pm W^\mp} = \frac{g}{2} \sum_i g_{H_i H^- W^+} \left(H_i \, \mathrm{i} \overleftrightarrow{\partial}_\mu H^- \right) W^{+,\mu} + \mathrm{h.c.}\,, \tag{3}$$

$$\mathcal{L}_{H_i \bar{b} b} = -\frac{g m_b}{2 m_W \cos\beta} \times \sum_i H_i \bar{b} \left[\mathrm{Re}\left(g_{H_i \bar{b} b}\right) - \mathrm{i}\,\mathrm{Im}\left(g_{H_i \bar{b} b}\right) \gamma_5 \right] b, \tag{4}$$

$$\mathcal{L}_{H^\pm t b} = \frac{g}{\sqrt{2} m_W} H^+ \bar{t} \times \left[m_t \cot\beta \frac{1-\gamma_5}{2} + m_b \tan\beta \frac{1+\gamma_5}{2} \right] b + \mathrm{h.c.}\,, \tag{5}$$

with the couplings

$$g_{H_i H^- W^+} = g^*_{H_i H^+ W^-} = O_{2i} \cos\beta - O_{1i} \sin\beta + \mathrm{i}\, O_{3i}\,, \quad g_{H_i \bar{b} b} = O_{1i} + \mathrm{i}\, O_{3i} \sin\beta\,, \tag{6}$$

where O_{ji} is the Higgs mixing matrix. In the real 2HDM, $H_i = \{h^0, H^0, A^0\}$ and the mixing matrix has the simple form

$$O_{ji} = \begin{pmatrix} -\sin\alpha & \cos\alpha & 0 \\ \cos\alpha & \sin\alpha & 0 \\ 0 & 0 & 1 \end{pmatrix}, \tag{7}$$

which gives purely real couplings for h^0 and H^0 and imaginary ones for A^0.

In the general CP-violating 2HDM all entries in the mixing matrix can be non-zero. The resulting mixing between CP-even and CP-odd Higgs states leads to complex couplings in general, which together with the propagators gives differences between the cross-sections for $b\bar{b} \to H^+W^-$ and $b\bar{b} \to H^-W^+$ in analogy to the $\mu^+\mu^- \to W^\pm H^\mp$ processes analyzed in [40]. However, it has to be kept in mind that the formalism we are using is simplified and only valid if at most one of the neutral Higgs propagators can be resonant. Otherwise one has to use the complete description [41, 42], which also takes into account non-diagonal propagator effects that arise from the mixing of two different Higgs bosons through higher order loops. Using the simplified formalism, the differential cross-sections for the two processes are [25, 40]

$$\begin{aligned} \frac{\mathrm{d}\sigma}{\mathrm{d}t}(b\bar{b} \to H^+W^-) = \frac{G_\mathrm{F}^2}{24\pi s} \Bigg\{ & \frac{m_b^2 \lambda\left(s, m_W^2, m_{H^\pm}^2\right)}{2\cos^2\beta} \\ & \times \sum_{i,j} g_{H_i H^- W^+} g^*_{H_j H^- W^+} S_{H_i} S^*_{H_j} \mathrm{Re}\left[g_{H_i \bar{b} b} g^*_{H_j \bar{b} b} \right] \\ & + \frac{1}{\left(t - m_t^2\right)^2} \left[m_t^4 \cot^2\beta (2m_W^2 + p_\perp^2) \right. \\ & \left. + m_b^2 \tan^2\beta \left(2 m_W^2 p_\perp^2 + t^2\right) \right] \\ & + \frac{m_b^2 \tan\beta}{\left(t - m_t^2\right)\cos\beta} \left[m_W^2 m_{H^\pm}^2 - s p_\perp^2 - t^2 \right] \\ & \times \sum_i \mathrm{Re}\left[g_{H_i H^- W^+} g_{H_i \bar{b} b} S_{H_i} \right] \Bigg\}, \end{aligned} \tag{8}$$

$$\begin{aligned} \frac{\mathrm{d}\sigma}{\mathrm{d}t}(b\bar{b} \to H^-W^+) = \frac{G_\mathrm{F}^2}{24\pi s} \Bigg\{ & \frac{m_b^2 \lambda\left(s, m_W^2, m_{H^\pm}^2\right)}{2\cos^2\beta} \\ & \times \sum_{i,j} g^*_{H_i H^- W^+} g_{H_j H^- W^+} S_{H_i} S^*_{H_j} \mathrm{Re}\left[g^*_{H_i \bar{b} b} g_{H_j \bar{b} b} \right] \\ & + \frac{1}{\left(t - m_t^2\right)^2} \left[m_t^4 \cot^2\beta \left(2 m_W^2 + p_\perp^2\right) \right. \\ & \left. + m_b^2 \tan^2\beta \left(2 m_W^2 p_\perp^2 + t^2\right) \right] \\ & + \frac{m_b^2 \tan\beta}{\left(t - m_t^2\right)\cos\beta} \left[m_W^2 m_{H^\pm}^2 - s p_\perp^2 - t^2 \right] \\ & \times \sum_i \mathrm{Re}\left[g^*_{H_i H^- W^+} g^*_{H_i \bar{b} b} S_{H_i} \right] \Bigg\}, \end{aligned} \tag{9}$$

where s and t are the ordinary Mandelstam variables of the hard process, and

$$\lambda(x, y, z) = x^2 + y^2 + z^2 - 2(xy + yz + zx)\,, \tag{10}$$

$$p_\perp^2 = \frac{\lambda\left(s, m_W^2, m_{H^\pm}^2\right) \sin^2\theta}{4s}\,, \tag{11}$$

with θ being the polar angle in the $2 \to 2$ CMS and

$$S_{H_i} = \frac{1}{s - m_{H_i}^2 + \mathrm{i} m_{H_i} \Gamma_{H_i}}\,. \tag{12}$$

In the remainder of this paper we focus on $H^\pm W^\mp$ production in the MSSM, with real and complex parameters, which is a special case of a type II 2HDM. The Higgs masses, widths, branching ratios and the mixing matrix of the neutral Higgs bosons in the MSSM can be calculated with programs such as FEYNHIGGS [47–50] and CPSUPERH [46], which include higher order corrections up to leading two-loop contributions, especially the Δm_b corrections.

As already alluded to, $H^\pm W^\mp$ production could potentially be used to determine the amount of CP-violation in the MSSM. In order to isolate the possible effects of CP-violation, a CP-odd rate asymmetry

$$A_{CP} = \frac{\sigma(pp \to H^+W^-) - \sigma(pp \to H^-W^+)}{\sigma(pp \to H^+W^-) + \sigma(pp \to H^-W^+)} \tag{13}$$

can be defined, where only interference terms contribute to the numerator:

$$\begin{aligned}
&\sigma(pp\to H^+W^-)-\sigma(pp\to H^-W^+)\\
&\propto \frac{\mathrm{d}\sigma}{\mathrm{d}t}(b\bar{b}\to H^+W^-)-\frac{\mathrm{d}\sigma}{\mathrm{d}t}(b\bar{b}\to H^-W^+)\\
&=\frac{G_\mathrm{F}^2}{12\pi s}\Bigg\{\frac{m_b^2\lambda\left(s,m_W^2,m_{H^\pm}^2\right)}{\cos^2\beta}\\
&\quad\times\sum_{i>j}\mathrm{Im}\left(g_{H_iH^-W^+}g^*_{H_jH^-W^+}\right)\mathrm{Im}\left(S_{H_i}S^*_{H_j}\right)\\
&\quad\times\mathrm{Re}\left(g_{H_i\bar{b}b}g^*_{H_j\bar{b}b}\right)\\
&\quad+\frac{m_b^2\tan\beta}{(t-m_t^2)\cos\beta}\left[m_W^2m_{H^\pm}^2-sp_\perp^2-t^2\right]\\
&\quad\times\sum_i\mathrm{Im}\left(g_{H_iH^-W^+}g_{H_i\bar{b}b}\right)\mathrm{Im}\left(S_{H_i}\right)\Bigg\}. \qquad (14)
\end{aligned}$$

From this expression it is clear that the conditions for obtaining large CP-asymmetries are quite subtle. Starting with the first term, which comes from the interference of two different s-channel amplitudes, we see that in this case large asymmetries can be obtained only if the phases in the propagators S_{H_i} make $\mathrm{Im}\left(S_{H_i}S^*_{H_j}\right)$ large and at the same time the Higgs mixing matrix O_{ij} leads to large factors from the couplings $\mathrm{Im}\left(g_{H_iH^-W^+}g^*_{H_jH^-W^+}\right)$ and $\mathrm{Re}\left(g_{H_i\bar{b}b}g^*_{H_j\bar{b}b}\right)$. Typically this means that the maximal asymmetry with one resonant propagator is of order Γ_{H_i}/m_{H_i}, modulo the coupling factors. In the more general case with several resonant propagators the formalism we are using is not sufficient as already noted. Looking at the second term in (14), which originates in the interference of one s-channel amplitude with the t-channel one, this can give an asymmetry of the order Γ_{H_i}/m_{H_i} if the s-channel amplitude is resonant, again modulo the coupling factor. However, in this case the coupling factor will make the asymmetry suppressed with $1/\tan\beta$ for large $\tan\beta$ compared to the asymmetry arising from the interference of two s-channel amplitudes.

2.2 Cross-section calculation

We have implemented [1] the two processes $b\bar{b}\to H^+W^-$ and $b\bar{b}\to H^-W^+$ as separate external processes to PYTHIA [52,53] in order to be able to analyze the rate asymmetry A_{CP}. In principle, the implementation in PYTHIA makes a generation of the complete final state possible, but for this first study we have chosen to stay on leading order parton level.

We use running b and t masses in the Yukawa couplings and a running electroweak coupling α_EW, all evaluated at the renormalization scale $\mu_\mathrm{R}=m_{H^\pm}+m_W$ using the leading order formulas implemented in PYTHIA. Numerically,

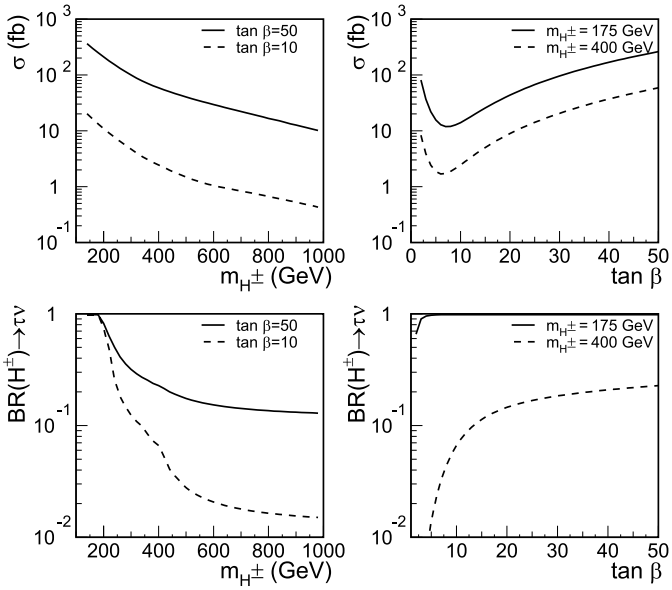

Fig. 2. The *left plots* show the ($b\bar{b}$ contribution to the) cross-section $\sigma\left(pp\to H^\pm W^\mp\right)$ at the LHC and the branching ratio $\mathrm{BR}\left(H^\pm\to\tau\nu_\tau\right)$ as a function of $m_{H^\pm}$ for $\tan\beta=50$ (*solid line*) and $\tan\beta=10$ (*dashed line*). The *right plots* show the cross-section and branching ratio as a function of $\tan\beta$ for $m_{H^\pm}=175$ GeV (*solid line*) and $m_{H^\pm}=400$ GeV (*dashed line*)

for $m_{H^\pm}=175$ (400) GeV the masses are $m_b=2.7$ (2.6) and $m_t=160$ (153) GeV. This leads to a reduction of the cross-section compared to the naive tree-level without running to about a third, which is in better agreement with the NLO calculation [31]. As factorization scale we use the average mass of the $H^\pm$ and the W, $\mu_\mathrm{F}=\frac{1}{2}(m_{H^\pm}+m_W)$, again for better agreement with NLO calculations. All other parameters are left at their default values in PYTHIA, for example, we use the CTEQ 5L [54] parton densities. We note that the main uncertainty in the b-quark parton density is not so much a question of which set is used, but rather of the precise value of the factorization scale. Varying the scale with a factor 2 up or down the cross-section changes with ±20%. This should be compared with the about ±5% uncertainty in the b density given for example by CTEQ65E [55] for relevant values of x and Q^2.[2] In addition the widths of the $H^\pm$ and W bosons are also included in the same way as in standard PYTHIA. In other words the $m_{H^\pm}$ and m_W masses vary according to Breit–Wigner distributions with varying widths meaning that for each mass the decay widths are recalculated based on the actually open decay channels.

For the calculation of the MSSM scenario and the corresponding Higgs masses, the Higgs mixing matrix O_{ji} and the branching ratios of $H^\pm$ we use FEYNHIGGS 2.2.10 [49]. From O_{ji} we then calculate the couplings $g_{H_iH^-W^+}$ and $g_{H_i\bar{b}b}$ according to (6).

[1] The fortran code for the $b\bar{b}\to H^+W^-$ and $b\bar{b}\to H^-W^+$ processes is available at [51].

[2] For this estimate we have used the online tool for pdf plotting and calculation at http://durpdg.dur.ac.uk/hepdata/pdf3.html.

Table 1. MSSM parameters for the maximal mixing scenario, $m_h^{\max}$, the less mixing scenario and the no mixing scenario in addition to $\tan\beta = 50$, $\mu = 200$ GeV, and $M_{\rm SUSY} = 1000$ GeV, as well as the resulting third generation squark masses

	MSSM parameters. All masses in GeV							
Scenario	A_t	A_b	M_2	$m_{\tilde{g}}$	$m_{\tilde{t}_1}$	$m_{\tilde{t}_2}$	$m_{\tilde{b}_1}$	$m_{\tilde{b}_2}$
Maximal mixing ($m_h^{\max}$)	2000	2000	200	800	820	1177	996	1012
Less mixing	1000	1000	200	800	922	1099	993	1012
No mixing	0	0	200	800	1014	1015	991	1014

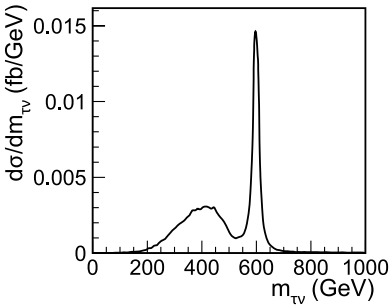

Fig. 3. Distribution of the invariant mass of the decay products (in our case $\tau\nu_\tau$) from the $H^{\pm}$ showing the off-shell enhancement of the cross-section for $m_{H^{\pm}} = 600$ GeV, resulting in $m_{H_{1,2,3}} = 136, 594, 594$ GeV. In this case the large width $\Gamma_{H^{\pm}}(m_{H^{\pm}}) = 20.3$ GeV means that the mass can fluctuate down to $m_{\tau\nu_\tau} + m_W < m_{H_i}$ which results in the broad peak seen to the left

Figure 2 shows the resulting total cross-section $\sigma(pp \to H^{\pm}W^{\mp})$ as well as the $H^{\pm}$ branching ratio into $\tau\nu_\tau$ as functions of the $H^{\pm}$ mass and $\tan\beta$ at the LHC. Here, and in the following unless otherwise noted, we have used a maximal mixing scenario, defined in Table 1.[3] At the same time, we have found that the cross-section depends very little on the mixing in the third generation squark sector. For example, for a mass of $m_{H^{\pm}} = 175$ GeV and $\tan\beta = 50$ the cross-section decreases from 260 fb to 257 fb in the no mixing scenario of Table 1.

Apart from the decreased cross-section due to the use of a running mass instead of the pole mass, our results also differ from, for example, the ones by [25] at large Higgs masses due to off-shell resonant enhancement. When the width of the $H^{\pm}$ is large, the mass of the decay products (in our case $\tau\nu_\tau$) can fluctuate down such that $m_{\tau\nu_\tau} + m_W < m_{H_i}$, giving rise to s-channel resonant production. This can be seen from the big broad peak in the $m_{\tau\nu_\tau}$ invariant mass spectrum shown in Fig. 3, which has been obtained for the following masses: $m_{H^{\pm}} = 600$ GeV, $m_{H_1} = 136$ GeV, $m_{H_2} = 594$ GeV, and $m_{H_3} = 594$ GeV. In turn this leads to an enhancement of the cross-section for large Higgs masses. The same effect can also be seen in the study of [26]. However, it is not clear to what extent this increase in the cross-section leads to a larger signal in the end, since the much wider peak could potentially be harder to see. This is especially true for the leptonic decays we are considering since here we can at best reconstruct the sum of the transverse momenta carried by neutrinos.

[3] Here $\tan\beta \equiv v_2/v_1$ denotes the ratio of the vacuum expectation values of the Higgs fields and μ is the Higgs/higgsino mass parameter. $M_{\rm SUSY}$ defines a common value of all squark and slepton soft SUSY breaking mass parameters M_Q^g, M_U^g, M_D^g, M_L^g and M_E^g, where $g = 1, 2, 3$ is the generation index. $X_t = A_t - \mu^* \cot\beta$ and $X_b = A_b - \mu^* \tan\beta$ describe the mixing in the third generation squark sector with the trilinear scalar couplings A_t and A_b. In the gaugino sector M_2 denotes the SU(2) soft SUSY breaking mass parameter, $m_{\tilde{g}}$ is the mass of the gluinos and the U(1) soft SUSY breaking mass parameter M_1 is fixed by the GUT relation $M_1/M_2 = 5/3\tan^2\theta_{\rm W}$.

3 Signal selection

In this section we explain the final signature analyzed in this paper, discuss background processes and define the cuts necessary to enhance the signal-to-background ratio.

The signal selection is based on the intermediate mass $m_{H^{\pm}} = 175$ GeV for $\tan\beta = 50$ in the maximal mixing scenario given in Table 1. Results based on this selection for other values of the mass and $\tan\beta$ as well as in other scenarios will be given in the next section.

3.1 Signature

As already mentioned, in this study we focus on associated $H^{\pm}W^{\mp}$ production with subsequent leptonic decays of the charged Higgs boson, $H^+ \to \tau^+\nu_\tau$ and hadronic decays of the W boson, $W^- \to \bar{q}q'$, $q = u, c$, $q' = d, s$. The decays $W^+ \to \tau^+\nu_\tau$ and $H^- \to \bar{c}s, \bar{c}b$ have not been included since the branching ratios for the latter are negligible compared to $H^+ \to \tau^+\nu_\tau$ for large $\tan\beta$. For simplicity we only consider hadronic decays of the τ lepton, $\tau \to \nu_\tau + \text{hadrons}$. The resulting signature thus consists of two light jets (j), one hadronic τ jet ($\tau_{\rm jet}$) and missing transverse momentum ($\not{p}_\perp$) carried away by the two neutrinos (one from the charged Higgs boson decay and one from the τ lepton decay):

$$2\text{j} + \tau_{\rm jet} + \not{p}_\perp \,.$$

Due to the two neutrinos escaping detection it is of course not possible to reconstruct the invariant mass of the charged Higgs boson in this decay mode. However, from $\not{p}_\perp$ and the transverse momentum of the τ jet, $p_{\perp\tau_{\rm jet}}$, the

Table 2. Set of basic cuts that define a signal region that corresponds to the sensitive region of a real detector and additional cuts that reduce the background according to the distributions in Fig. 5 as well as suppress QCD background and detector misidentifications

Basic cuts	Additional cuts [all in GeV]
$\lvert\eta_{\tau_{\rm jet}}\rvert < 2.5$	$p_{\perp\tau_{\rm jet}} > 50$, $\not{p}_\perp > 50$
$\lvert\eta_j\rvert < 2.5$	$70 < m_{\rm jj} < 90$
$\Delta R_{\rm jj} > 0.4$	$m_\perp > 100$
$\Delta R_{\tau_{\rm jet}j} > 0.5$	$p_{\perp\rm hj} > 50$, $p_{\perp\rm sj} > 25$
$p_{\perp\rm jet} > 20\,\rm GeV$	

transverse mass[4]

$$m_\perp = \sqrt{2p_{\perp\tau_{\rm jet}}\not{p}_\perp[1-\cos(\Delta\phi)]} \qquad (15)$$

can be calculated, where $\Delta\phi$ is the azimuthal angle between $p_{\perp\tau_{\rm jet}}$ and $\not{p}_\perp$. If there is a detectable charged Higgs boson it will show up as a peak in this distribution with the upper edge of the peak given by the mass of the charged Higgs boson.

3.2 Background

The dominant irreducible SM background for our signature $2{\rm j}+\tau_{\rm jet}+\not{p}_\perp$ arises from $W+2$ jets production which we have simulated with help of the package ALPGEN [56]. The program calculates the exact matrix elements on tree-level for the $2{\rm j}+\tau+\nu_\tau$ final state. In this way it includes not only $W+2$ jets production as well as W pair production, but also contributions where the τ lepton and the neutrino do not arise from the decay of a (virtual) W boson. The obtained cross-sections and distributions of momenta, invariant masses etc. have been cross-checked with Madgraph [57–59].

As a further precaution we have also simulated another irreducible background, namely $WZ+2$ jets production with $Z\to\nu\nu$ using ALPGEN, which typically has a larger missing transverse momentum. However, we have found that this process contributes less than 3% to the overall background after appropriate cuts (see Table 2) have been applied. So even though the tails of the $p_\perp$ and $m_\perp$ distributions are slightly harder compared to the $W+2$ jets background, it is still safe to neglect the $WZ+2$ jets background for this study.

The importance of using the complete matrix element for the signature we are considering, and not just the Wjj approximation, can be seen in Fig. 4. The figure shows the invariant mass $m_{\tau\nu_\tau}$ of the τ and ν_τ system generated with ALPGEN compared to the W mass from PYTHIA in $W+$ jet production, which has a normal Breit–Wigner distribution with varying width. Of special interest here is the tail

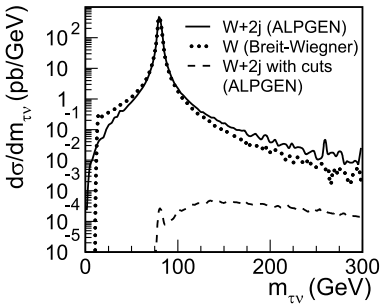

Fig. 4. Invariant mass $m_{\tau\nu_\tau}$ of the τ and ν_τ system generated with ALPGEN (*solid line*) compared to the W mass from PYTHIA in $W+$ jet production (*dotted line*), which has a normal Breit–Wigner distribution with varying width. The distributions have been normalized to the same height. Also shown is the $m_{\tau\nu_\tau}$ distribution generated with ALPGEN after applying the cuts defined in Table 2 (*dashed line*)

for large invariant masses $m_{\tau\nu_\tau}$ and we note that there is a factor of 2 difference between the two approaches in this tail. To illustrate the invariant mass range of relevance in our case we also show $m_{\tau\nu_\tau}$ generated with ALPGEN after all event selection cuts (see Table 2) have been applied. This also shows that the SM background can be considerably reduced by appropriate cuts, which will be discussed in the next subsection.

3.3 Cuts

Our study is performed at parton level, without any parton showering or hadronization. Instead the momenta of the jets are smeared as a first approximation to take these, as well as detector effects, into account. The only exception is that for both signal and background TAUOLA [60, 61] has been used to perform the decay of the τ lepton into a hadronic jet plus a neutrino. The use of TAUOLA also makes it possible to take into account the differences in the decay characteristics of the τ lepton depending on whether it comes from a charged Higgs bosons with spin 0 or a W boson with spin 1. This difference can, at least in principle, also be used to discriminate against backgrounds [9, 11, 62, 63] as discussed below.

We distinguish between the two jets by calling them hard (with momentum $p_{\rm hj}$) and soft ($p_{\rm sj}$) according to the larger and smaller value of their transverse momentum $p_\perp$, respectively. We have done a Gaussian smearing of the measurable momenta $p_{\tau_{\rm jet}}$, $p_{\rm hj}$ and $p_{\rm sj}$ and then calculated $\not{p}_\perp$. The smearing is done preserving the direction of the momenta and the width of the smearing is defined as $\sigma[\rm GeV] = \sqrt{\frac{a^2}{p_{\perp}[\rm GeV]}+b^2}$ with $a=0.60$ and $b=0.02$.

Our set of basic cuts, see Table 2, is defined according to the coverage and resolution of a realistic detector. First we require that the pseudorapidity of the $\tau_{\rm jet}$ and the light jets are in the range $-2.5<\eta<2.5$. A further cut requires a minimal distance $\Delta R_{\rm jj}>0.4$ and $\Delta R_{\tau_{\rm jet}{\rm j}}>0.5$ between two respective jets to allow for their separation.

[4] Strictly speaking this is not the transverse mass, since there are two neutrinos in the decay chain of the charged Higgs boson we are considering. Even so the characteristics of this mass are very similar to those of the true transverse mass.

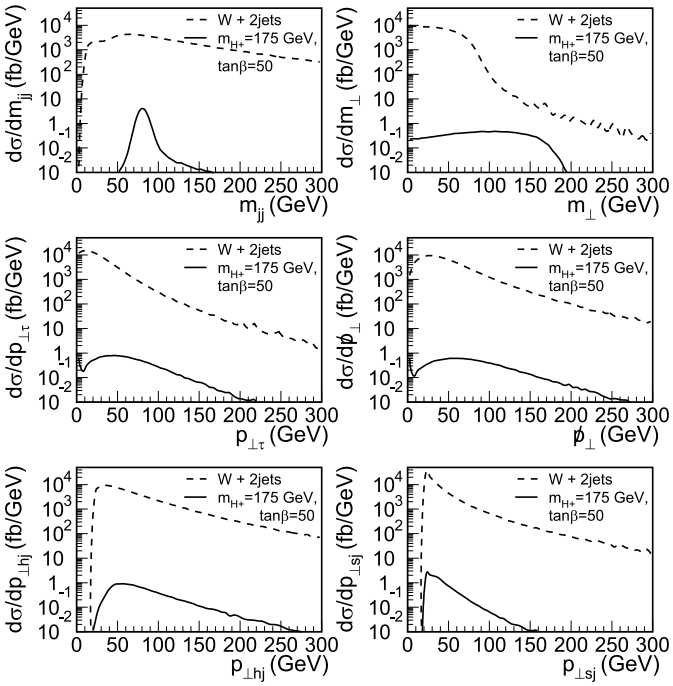

Fig. 5. *Top row*: $m_{\rm jj}$ and $m_\perp$ distributions for signal (*solid*), and background (*dashed*). *Middle row*: $p_\perp$ distributions for $\tau_{\rm jet}$ and $\not{p}$. *Bottom row*: $p_\perp$ distributions for the hard and soft light jet. In all plots the basic cuts of Table 2 have been applied

Finally we require a minimum $p_\perp > 20$ GeV for all jets. Figure 5 shows the resulting $m_{\rm jj}$, $m_\perp$ distributions and the $p_\perp$ distributions for all jets and the missing transverse momentum for the signal and background after these basic cuts.

Based on the shape of the signal and background in Fig. 5 we define further cuts. These cuts are used to reduce the background, while keeping as much signal as possible. It can be seen that a cut $70\,\text{GeV} < m_{\rm jj} < 90\,\text{GeV}$ will be very efficient since the signal is peaked around the W mass, whereas the background is almost flat. A cut $m_\perp > 100\,\text{GeV}$ will also remove a large part of the background. Increasing this cut leads to smaller $S/\sqrt{B}$ for $m_{H^\pm} = 175\,\text{GeV}$, yet might be useful for higher $m_{H^\pm}$. The signal peak has a soft upper edge, so for Higgs masses below 125 GeV it would be very hard to see the signal, since the background increases dramatically in this region. To further reduce the background the cuts $p_{\perp\rm hj} > 50\,\text{GeV}$ and $p_{\perp\rm sj} > 25\,\text{GeV}$ are defined. In addition, we apply the cuts $p_{\perp\tau_{\rm jet}} > 50\,\text{GeV}$ and $\not{p}_\perp > 50\,\text{GeV}$, similarly to [34], in order to reduce the QCD background and the effects of detector misidentifications although we have not simulated these effects explicitly. Since these cuts may be too soft we will also show results for the harder cuts $p_{\perp\tau_{\rm jet}} > 100\,\text{GeV}$ and $\not{p}_\perp > 100\,\text{GeV}$, which have been used for example in [15].

As mentioned above the τ-jet properties of the signal and background are also different due to the difference in spin of the $H^\pm$ and W bosons. The relevant measure is the ratio, R, between the transverse momentum of the leading charged π, $p_{\perp\pi}$, and the total transverse momentum of the

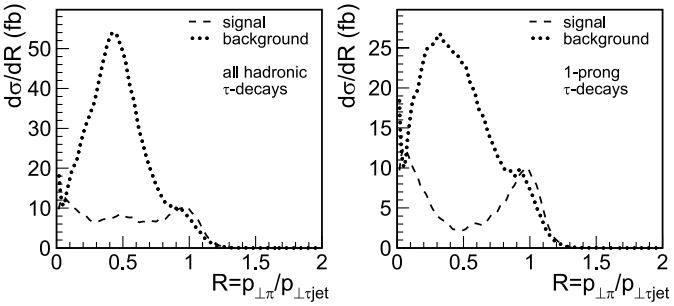

Fig. 6. Comparison of $R = p_{\perp\pi}/p_{\perp\tau_{\rm jet}}$ between signal (for $m_h^{\rm max}$ with $m_{H^\pm} = 175\,\text{GeV}$ and $\tan\beta = 50$) and background. The *left plot* is for all events and the *right* one for 1-prong events. The *dashed* (*dotted*) curve denotes signal (background)

τ jet,

$$R = \frac{p_{\perp\pi}}{p_{\perp\tau_{\rm jet}}}\,. \tag{16}$$

We assume that $p_{\perp\pi}$ is measured in the tracker independently of the transverse momentum of the τ-jet and in order to take into account the tracker performance we apply Gaussian smearing on $1/p_{\perp\pi}$ with

$$\sigma\left(\frac{1}{p_{\perp\pi}}\right)[\text{TeV}^{-1}] = \sqrt{0.52^2 + \frac{22^2}{(p_{\perp\pi}[\text{GeV}])^2 \sin\theta_\pi}}\,, \tag{17}$$

where θ_π is the polar angle of the π [64].

Having applied all the cuts outlined above, the resulting distribution of R is shown in Fig. 6, both when keeping all hadronic τ decays as well as only selecting 1-prong decays. As can be seen from the figure, the differences between the signal and background is clear in both cases. Even so, we have found that applying cuts on R in either of the two cases does not lead to an improved overall significance $S/\sqrt{B}$ compared to the case when all hadronic τ decays are kept and no cut on R is applied. (When selecting only 1-prong events a cut $R > 0.8$ turns out to be advantageous, but the overall significance still drops compared to keeping all hadronic τ decays.) At the same time it should be kept in mind that these conclusions may change when making a complete simulation of the final state including parton showers and hadronization as well as a full detector simulation. It may also be possible to enhance the use of τ-polarization by considering the 3-prong decays separately and looking at the sum of the transverse momenta of the like-sign pair instead of that of the leading charged pion [63].

In Table 2 all basic and additional cuts are summarized and in Table 3 is shown how applying the different additional cuts one after the other affects the integrated cross-section. The signal is given for the $m_h^{\rm max}$ scenario in Table 1 with a charged Higgs mass of 175 as well as 400 GeV and $\tan\beta = 50$. We have used an integrated luminosity of $300\,\text{fb}^{-1}$ and a τ detection efficiency of 30% to calculate $S/\sqrt{B}$. Finally, we note that when the charged Higgs mass

Table 3. The effect of the different cuts on the integrated cross-section for background (σ_b) and signal (σ_s) in the $m_h^{\max}$ scenario with $m_{H^\pm} = 175$ and 400 GeV for $\tan\beta = 50$ (see Table 1) as well as the number of signal events S and the significance $S/\sqrt{B}$ assuming an integrated luminosity of 300 fb^{-1} and a τ detection efficiency of 30%

		$m_{H^\pm} = 175$ GeV			$m_{H^\pm} = 400$ GeV		
Cut [all in GeV]	σ_b (fb)	σ_s (fb)	S	$S/\sqrt{B}$	σ_s (fb)	S	$S/\sqrt{B}$
Basic cuts	560 000	55	4900	0.7	3.3	300	0.04
$p_{\perp\tau_{\rm jet}} > 50$, $\not{p}_\perp > 50$	22 000	25	2200	1.6	2.7	240	0.2
$70 < m_{\rm jj} < 90$	1700	21	1900	5	2.2	200	0.5
$m_\perp > 100$	77	15	1400	16	2.1	190	2.3
$p_{\perp\rm hj} > 50$, $p_{\perp\rm sj} > 25$	28	9.3	840	17	1.5	135	2.6

is large it can be advantageous to use the harder set of cuts $p_{\perp\tau_{\rm jet}} > 100$ GeV and $\not{p}_\perp > 100$ GeV as illustrated below. In order to get a rough estimate of how important higher order corrections can be on the resulting significances we consider the following worst case scenario. Assuming the total uncertainty in the signal as well as background to be a factor 1.5, then the significances in Table 3 would in the worst case be reduced with a factor 1.8.

4 Results

In this section we present the results of our analysis in the MSSM with real and complex parameters as well as in special scenarios with large mass splittings giving resonant enhancement of the signal.

4.1 MSSM with real parameters

Unless otherwise noted we use in the following a standard maximal mixing scenario, $m_h^{\max}$, with $X_t = 2M_{\rm SUSY}$ as defined in [65]. All SUSY parameters needed as input to calculate the Higgs masses and mixing matrix with FEYNHIGGS are given in Table 1. For the electroweak parameters, $m_t = 178$ GeV, $m_b = 4.7$ GeV, $m_W = 80.426$ GeV, and $m_Z = 91.187$ GeV have been used. $G_{\rm F}$ has been calculated from the running $\alpha_{\rm EW}$ as $G_{\rm F} = \frac{\pi\alpha_{\rm EW}}{\sqrt{2}\sin^2\theta_{\rm W} m_W^2}$. We have checked that the impact of using a lower $m_t = 172$ GeV on the signal rates and distributions is small compared to the uncertainties from higher order effects and can safely be neglected. This also applies to the branching ratio Br$(H^+ \to \tau^+\nu_\tau)$, which in the case of $m_{H^\pm} = 400$ GeV is reduced from 22.7 to 22.0%.

The mass and $\tan\beta$ dependence of the cross-section after all cuts of Table 2 are shown in Fig. 7 as solid curves whereas dashed curves denote the cross-section for the harder cuts $p_{\perp\tau_{\rm jet}} > 100$ GeV and $\not{p}_\perp > 100$ GeV. The left plot is for $\tan\beta = 50$, whereas in the right plot we have used $m_{H^\pm} = 175$ GeV (400 GeV) for the solid (dashed) line. The horizontal lines indicate the cross-section needed for $\frac{S}{\sqrt{B}} = 5$. Using this criterion to define a detectable signal we see that this would indeed be the case for $\tan\beta \gtrsim 30$ if $m_{H^\pm} = 175$ GeV and for 150 GeV $\lesssim m_{H^\pm} \lesssim$ 300 GeV if $\tan\beta = 50$ with the softer cuts $p_{\perp\tau_{\rm jet}} > 50$ GeV and $\not{p}_\perp >$ 50 GeV, whereas with the harder cuts $\tan\beta$ has to be larger than at least 50 in order to have a detectable signal.

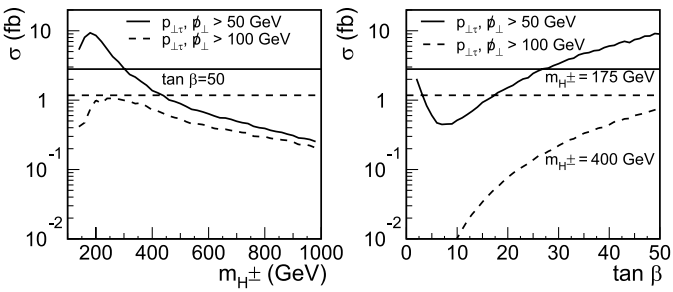

Fig. 7. $H^\pm$ mass and $\tan\beta$ dependence of the integrated cross-section in the $m_h^{\max}$ scenario. *Solid curves* are with all cuts of Table 2, and *dashed curves* are with the harder cuts $p_{\perp\tau_{\rm jet}} >$ 100 GeV and $\not{p}_\perp > 100$ GeV. The *horizontal lines* correspond to $\frac{S}{\sqrt{B}} = 5$

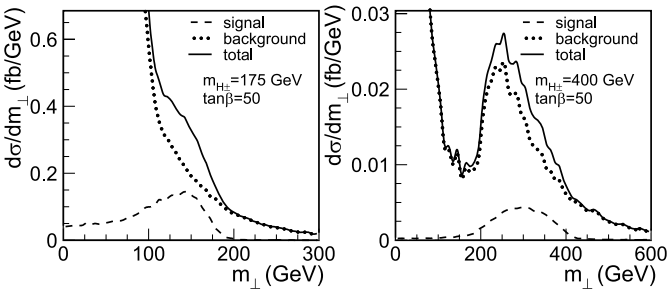

Fig. 8. Comparison of the $m_\perp$ distribution between the signal in the $m_h^{\max}$ scenario with $\tan\beta = 50$ and $m_{H^\pm} = 175$ GeV (*left*) as well as $m_{H^\pm} = 400$ GeV (*right*) together with the respective backgrounds with all cuts of Table 2 (for the high mass the harder cuts $p_{\perp\tau_{\rm jet}} > 100$ GeV and $\not{p}_\perp > 100$ GeV are used). The *dashed curve* denotes the signal and the *dotted* one the background, whereas the *solid curve* is the sum of the two

Figure 8 shows the resulting $m_\perp$ distribution for a charged Higgs mass of 175 GeV as well as 400 GeV in the case $\tan\beta = 50$ compared to the background after all cuts in Table 3 have been applied. In the high mass case the harder cuts $p_{\perp\tau_{\rm jet}} > 100$ GeV and $\not{p}_\perp > 100$ GeV are used but all the other cuts are the same. For an integrated luminosity of 300 fb^{-1} and a τ detection efficiency of 30% we get $S/\sqrt{B} = 17$ for $m_{H^\pm} = 175$ GeV and $S/\sqrt{B} = 3.2$ for $m_{H^\pm} = 400$ GeV. (The latter result is slightly bet-

ter than what would have been obtained with the softer cuts $p_{\perp\tau_{\rm jet}} > 50\,\text{GeV}$ and $\not{p}_{\perp} > 50\,\text{GeV}$.) Here, and in all following calculations of $S/\sqrt{B}$, we have used the cut $m_{\perp} > 100\,\text{GeV}$ to get S and B. In the high mass case $S/\sqrt{B}$ could in principle be improved by imposing a harder cut on $m_{\perp}$, as can be seen from the figure, but not much. Also the possible use of upper cuts $m_{\perp} < 200\,\text{GeV}$ ($m_{\perp} < 500\,\text{GeV}$) for $m_{H^{\pm}} = 175\,\text{GeV}$ ($m_{H^{\pm}} = 400\,\text{GeV}$) only marginally improves $S/\sqrt{B}$ from 17 (3.2) to 19 (3.3). In the same figure we also see that the harder cuts create a fake peak in the background, which could make it more difficult to tell if there is a signal. This fake peak appears since the τ and ν_{τ} are mostly produced back to back in the $W + 2$ jets process. Using the harder cuts $p_{\perp\tau_{\rm jet}} > 100\,\text{GeV}$ and $\not{p}_{\perp} > 100\,\text{GeV}$ to reduce QCD background and detector misidentifications, the significance for $m_{H^{\pm}} = 175\,\text{GeV}$ and $\tan\beta = 50$ is reduced to $S/\sqrt{B} = 3.1$. However, in this case using a upper cut $m_{\perp} < 200\,\text{GeV}$ is beneficial, leading to a significance of $S/\sqrt{B} = 6.4$. This means that if the softer cuts $p_{\perp\tau_{\rm jet}} > 50\,\text{GeV}$ and $\not{p}_{\perp} > 50\,\text{GeV}$ are sufficient to suppress the QCD background, these are clearly to be preferred.

4.2 MSSM with complex parameters

In the general MSSM many parameters can be complex. However, our signal process, analyzed as described in Sect. 2, is only affected by CP-violation in the neutral Higgs sector because of the neutral Higgs bosons exchanged in the s-channel. The leading contributions to the CP-violation in the neutral Higgs sector arise from loops of the scalar top and (to a lesser extend) of the scalar bottom sector where the possibly complex Higgs/higgsino mass parameter μ and the trilinear scalar couplings A_t and A_b are dominant. Furthermore, in constrained MSSM scenarios implying universality conditions at the GUT scale and rotating away all unphysical phases with help of U(1) symmetries of the theory, only two phases remain, the phase of μ and a common phase for the trilinear couplings [38, 39]. Hence, we concentrate in the following on the phases ϕ_{μ} and ϕ_{A_t} of μ and A_t, respectively, which have the largest effect on the neutral Higgs sector and thus possibly affect our signal, assuming $\phi_{A_b} = \phi_{A_\tau} = \phi_{A_t}$. We have varied ϕ_{μ} and ϕ_{A_t} independently in the range $-\pi < \phi < \pi$ in order to investigate the phase dependence of our signal. However, in the maximal mixing scenario as well as in scenarios with less and no mixing in the third generation squark sector, see Table 1, we find only small ($\sim 5\%$) ϕ_{μ} and ϕ_{A_t} dependencies of the total cross-section as can be seen in Fig. 9.

The small effects of the phases in these MSSM scenarios are basically due to the neutral Higgs bosons having quite similar masses $\left(m^2_{H_i} - m^2_{H_j} \ll (m_{H^{\pm}} + m_W)^2 - m^2_{H_i}\right)$ and small widths with the latter also being true for the charged Higgs boson. Bearing in mind that $s \gtrsim \left(m_{H^{\pm}} + m_W\right)^2$, the propagators, $S_{H_i} = 1/\left(s - m^2_{H_i} + \mathrm{i} m_{H_i}\Gamma_{H_i}\right)$, in (8) and (9) are all of similar size and approximately real. Therefore, as a first approximation, they can be put in front of the sum over the different Higgs bosons. The remaining sums of coupling factors then reduce to simple numbers, the first to $2\sin^2\beta$ and the second to $-2\sin\beta$, irrespective of the entries in the Higgs mixing matrix, O_{ji}. Thus, unless we have large differences in the masses of the neutral Higgs bosons, the effect from the phases via the couplings is small. The phase dependence also enters indirectly via the Higgs masses, which typically have a large dependence on the phases. It turns out that in the scenarios we are considering the total cross-section has an almost linear dependence on the mass of the heaviest neutral Higgs boson, and the phase dependence from the masses is much larger than that from the couplings.

Figure 9 also shows the allowed regions from the following precision measurements, the anomalous magnetic moment of the muon, a_{μ}, the ρ parameter, $\delta\rho_0$ and the electric dipole moments (EDMs) of e, n and Hg. The experimental value of a_{μ} from [66] is

$$a_{\mu}^{\rm exp} = 11\,659\,208.0 \pm 5.8 \times 10^{-10} \tag{18}$$

and the theoretical value determined using the e^+e^- data from [67] is

$$a_{\mu}^{\rm SM} = 11\,659\,184.1 \pm 8.0 \times 10^{-10}. \tag{19}$$

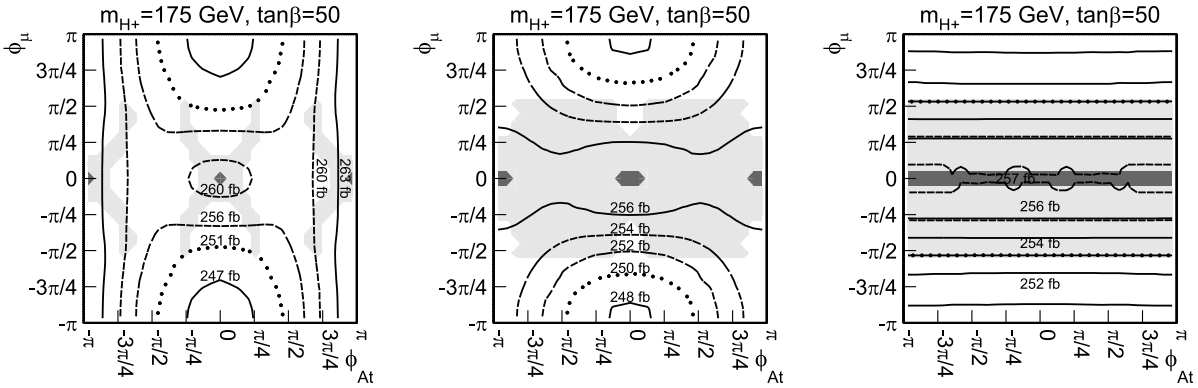

Fig. 9. Total cross-section as a function of ϕ_{μ} and ϕ_{A_t} in the maximal mixing scenario (*left*), the less mixing scenario (*middle*) and the no mixing scenario (*right*). The *light shaded areas* are in agreement with the constraints from a_{μ} and $\delta\rho_0$ and the *dark shaded* ones are also in agreement with the constraints from EDMs

Table 4. MSSM parameters for the resonant scenario as well as the range for the scan of parameters together with the stepsize

	MSSM parameters. All masses in GeV											
	$m_{H^{\pm}}$	$\tan\beta$	μ	M_L^3	M_E^3	M_Q^3	M_U^3	M_D^3	A_t	A_b	M_2	$m_{\tilde{g}}$
Resonant scen.	175	11	3300	500	500	250	250	400	0	0	500	500
Scan min	100	1	1800	500	500	150	150	150	0	0	500	500
Scan max	450	40	3300	500	500	650	650	650	0	0	500	500
Scan stepsize	25	1	250	–	–	50	50	50	–	–	–	–

Based on these values we use the following 2σ range for the difference:

$$-3.7\times10^{-10} < \Delta a_\mu < 51.5\times10^{-10}\,. \tag{20}$$

The experimentally allowed range of $\delta\rho_0$ is [2]

$$-0.0010 < \delta\rho_0 < 0.0025\,, \tag{21}$$

whereas we use the following upper limits on the EDMs [68–70]

$$|d_e| < 1.6\times10^{-27}\,, \tag{22}$$
$$|d_n| < 6.3\times10^{-26}\,, \tag{23}$$
$$|d_{\rm Hg}| < 2.1\times10^{-28}\,. \tag{24}$$

In order to calculate a_μ, $\delta\rho_0$, $|d_e|$, $|d_n|$ and $|d_{\rm Hg}|$ in our scenarios and to analyze their dependence on the phases of μ and A_t we have used FEYNHIGGS 2.2.10, where, however, it is important to keep in mind that the EDM routines have not yet been fully tested. As can be seen from Fig. 9 the restrictions from the precision measurements are very severe. The bound on a_μ effectively removes the region with $|\phi_\mu| \gtrsim \pi/2$ and in the remaining region only the light shaded areas are consistent with the $\delta\rho_0$ bound. Finally the darker shaded areas are those consistent also with the EDMs. Hence only small variations from phase zero or π are allowed.

The constraints from the EDMs are very strong in constrained MSSM scenarios, allowing only small values of the phases, especially of ϕ_μ. However, in unconstrained SUSY they are rather model dependent, permitting in general larger phases. For example, due to cancellations between different SUSY contributions to the EDMs or in SUSY models with heavy sfermions in the first two generations larger phases may be allowed [71–79]. Recently it has been pointed out that for large trilinear scalar couplings A, the phases $\phi_\mu \sim O(1)$ can be compatible with the bounds on d_e, d_n and $d_{\rm Hg}$ [80]. Furthermore the restrictions on the phases may also disappear if lepton flavor violating terms in the MSSM Lagrangian are included [81]. In conclusion this means that large phases cannot be ruled out and therefore we analyze the full range of the phases to determine possible effects.

To see the dependence of the allowed regions on the chosen SUSY scenario we show in Fig. 9 also the results for the less mixing and no mixing scenarios. In the less mixing scenario the constraints from $\delta\rho_0$ are less severe but the EDMs still give hard constraints, whereas for the no mixing scenario we get a complete band around $\phi_\mu = 0$. Finally we have also checked that similar results are obtained for $\tan\beta = 10$.

In the MSSM scenarios studied in this section the CP-odd rate asymmetry, (13), is always quite small, $|A_{CP}| \lesssim 0.3\%$. This due to the fact that in order to get a large asymmetry the effects from the absorptive phases in the Higgs propagators, S_{H_i}, as well as the phases in the couplings have to be large. On the contrary, in the scenarios considered here the phases in S_{H_i} are always quite small and at the same time the mixing between the neutral Higgs bosons is also typically small, resulting in small asymmetries. In order to get a non-negligible asymmetry one needs large phases from at least one of the propagators and at the same time large mixing between the neutral Higgs bosons, which seems difficult to achieve in the MSSM. In more general 2HDMs, large asymmetries should be possible in scenarios with two resonant neutral Higgs bosons in the s-channel and large mixing, although this remains to be verified.

4.3 Resonant scenarios

In SUSY parameter regions with $|\mu|, |A_t|$, or $|A_b| > 4M_{\rm SUSY}$ the dominant terms of the one-loop corrections to the quartic couplings in the Higgs sector [39] can induce a large mass splitting between the charged and neutral Higgs bosons [82, 83]. For example, in the scenario given in Table 4, the CP-odd Higgs is 80 GeV heavier than the charged Higgs, allowing for resonant production in the s-channel.

In order to examine the perturbative stability of this scenario with very large one-loop corrections to the mass of the CP-odd Higgs boson we list in Table 5 the masses of the Higgs bosons calculated with FEYNHIGGS[5] at tree-level, at one-loop order, and with all available corrections. For comparison, the Higgs masses in the maximal mixing scenario are also given. From the table it is clear that the higher order corrections have a much smaller impact than the leading ones, suggesting that the perturbative expansion is under control. We have also verified that similarly large mass splittings are obtained with CPSUPERH using all available corrections although not in precisely the same

[5] We have added the partial decay width $\Gamma(H_i \to H^{\pm}W^{\mp})$ to the calculation of Γ_{H_i} in FEYNHIGGS.

Table 5. Masses of the Higgs bosons in the maximal mixing and resonant scenarios, calculated with FEYNHIGGS at tree level, at one-loop order and using all available corrections

	$m_h^{\max}$	Resonant scenario		
	full	tree-level	1-loop	full
m_{h^0}	136 GeV	89 GeV	95 GeV	118 GeV
m_{H^0}	151 GeV	157 GeV	188 GeV	168 GeV
m_{A^0}	**151 GeV**	**155 GeV**	**246 GeV**	**258 GeV**
$m_{H^\pm}$	**175 GeV**	**175 GeV**	**175 GeV**	**175 GeV**

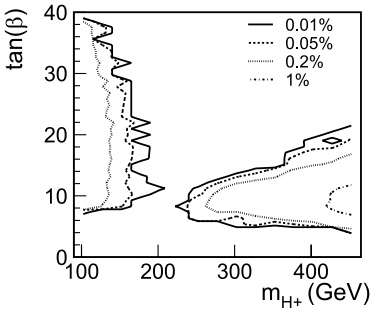

Fig. 10. Contour plot of the relative number of resonant scenarios to physical scenarios in each point. The *lines* are 0.01%, 0.05%, 0.2% and 1%. The region around $\tan\beta \approx 8$ contains more physical scenarios than the upper region leading to a total of 0.2% resonant scenarios

parameter points. The latter feature is due to this kind of resonant scenarios being rather fine-tuned and therefore sensitive to differences in the implementation and approximations used in the two programs.

To get an indication of how fine-tuned this kind of resonant scenario is, we have performed a scan over the relevant parameters as shown in Table 4. Defining a resonant scenario via the relation $m_A > m_{H^\pm} + m_W$, there is in fact a large range in both $\tan\beta$ and $m_{H^\pm}$ where such scenarios are found, as can be seen in Fig. 10. In each $\tan\beta$ and $m_{H^\pm}$ point about 9300 different scenarios are tested. On average about one half of these correspond to physical scenarios and in turn about 0.2% of the latter give resonant conditions, which illustrates the level of fine-tuning in these scenarios. The dependence on $\tan\beta$ and $m_{H^\pm}$ is illustrated in Fig. 10. At the same time, these scenarios typically have relatively low squark masses, so for large $m_{H^\pm}$ ($\gtrsim 200\,\text{GeV}$) the decay to squarks becomes dominant and thus the specific analysis we present here is not suitable. At the same time, in scenarios with light squarks there may also be a resonant enhancement in the gluon initiated channel from squark loops as already discussed above. This occurs if the sum of the squark masses is close to threshold. In addition, it is also possible in this case to have enhancement from the s-channel resonance. Thus in the rare situation that both these effects occur simultaneously, without opening the decay channel of the charged Higgs into squarks, the signal could in fact be enhanced. Finally, we note that the study of resonant scenarios also illustrates what could happen in a general

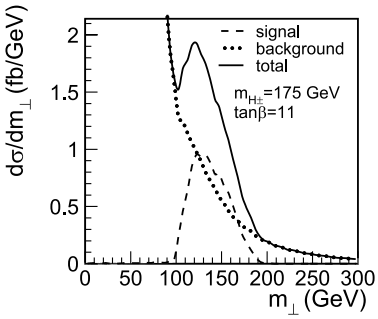

Fig. 11. Comparison of $m_\perp$ distribution between signal (for the resonant scenario with $m_{H^\pm} = 175\,\text{GeV}$ and $\tan\beta = 11$ given in Table 4) and background with all cuts of Table 2 except $p_{\perp\text{hj}} > 50\,\text{GeV}$ and $p_{\perp\text{sj}} > 25\,\text{GeV}$. The *dashed* (*dotted*) *curve* denotes signal (background) and the *solid curve* is signal and background combined

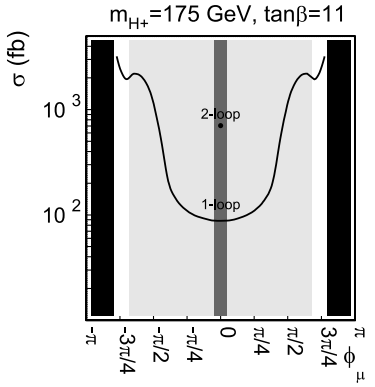

Fig. 12. Total cross-section, with the Higgs masses etc. calculated to one-loop, as a function of ϕ_μ for the resonant scenario. For comparison the result with all available corrections for $\phi_\mu = 0$ is also shown (labeled 2-loop). The *light shaded areas* are in agreement with the constraints from a_μ and $\delta\rho_0$ and the *dark shaded* ones are also in agreement with the constraints from EDMs. In the *black areas* numerical instabilities occurred in the calculation of the Higgs masses and mixing matrix

2HDM, where the masses are more or less independent parameters.

In case of resonant production, the $H^\pm$ and W bosons are produced with typically small transverse momenta. Thus it is favorable to loosen the cuts on the light jets from the W. Applying the basic and additional cuts from Table 2, except the cuts $p_{\perp\text{hj}} > 50\,\text{GeV}$ and $p_{\perp\text{sj}} > 25\,\text{GeV}$ on the light jets, we get an integrated cross-section of 52 fb for a charged Higgs boson mass of 175 GeV in the resonant scenario given in Table 4. Figure 11 shows the resulting $m_\perp$ distribution compared to the background. With an integrated luminosity of $300\,\text{fb}^{-1}$ and a τ detection efficiency of 30% we get a significance $S/\sqrt{B} = 56$. For comparison, if we apply the harder cuts $p_{\perp\tau_{\text{jet}}} > 100\,\text{GeV}$ and $\not{p}_\perp > 100\,\text{GeV}$ in this resonant case, the significance is reduced drastically to $S/\sqrt{B} = 0.2$ due to the typically small transverse momentum of the $H^\pm$ boson. Thus, in the case of harder cuts the resonantly enhanced cross-section is only of use

if $m_{H^\pm}$ is large enough such that $m_{H^\pm}/2$ is well above 100 GeV.

Finally, we have also tried to investigate the phase dependence of the cross-section in this resonant scenario. Figure 12 shows the dependence of the cross-section on ϕ_μ, where the Higgs masses, couplings and widths have been calculated with FEYNHIGGS at one-loop accuracy[6]. Note that the phase ϕ_{A_t} is irrelevant in this scenario because $|A_t| = 0$. For comparison, the figure also shows the result with all available corrections in the case $\phi_\mu = 0$. The very large phase dependence is due to the fact that the production goes from non-resonant to resonant when varying the phase. More specifically, as can be seen in Table 5 we get $m_A = m_{H_3} = 246$ GeV for $\phi_\mu = 0$ in the one-loop case, which is below the resonant threshold, whereas $m_{H_3} = 342$ GeV for the largest values of ϕ_μ where we got a stable result, which is clearly in the resonant regime. Even in these resonant cases, the width of the H_3 is typically small, $\Gamma/m \lesssim 0.02$, and consequently the CP-asymmetry is also small. However, we have not been able to make a more thorough study of the sensitivity to these phases due to numerical instabilities, nor have we searched for resonant scenarios with large Γ/m as well as large mixings, since this requires a dedicated study.

5 Summary and conclusions

In this paper we have studied the viability of detecting charged Higgs bosons produced in association with W bosons at the upcoming LHC experiments. Since our study is of exploratory character we have stayed on the parton level, although with appropriate smearing of momenta, and we leave the inclusion of parton showering, hadronization, full simulation of the detector, etc. for future studies. In the same vain we have not tried to include any higher order corrections in the production cross-section. The only exception is that we use running quark masses in the Yukawa couplings, which gives a cross-section that is almost a factor three smaller compared to when using the pole mass, in agreement with NLO QCD [31]. Other higher order corrections on the production cross-section, such as the choice of the factorization scale, are expected to be $\mathcal{O}(10\%–20\%)$.

As we have shown in this paper, using the leptonic decay of the charged Higgs boson and hadronic W decay, giving rise to the signature $\tau_{\text{jet}}\not{p}_\perp + 2$ jets, it is possible to design appropriate cuts against the irreducible standard model background from $W + 2$ jets production. This is in contrast to earlier studies using hadronic decays of the charged Higgs bosons, which were found to suffer from too large irreducible backgrounds due to $t\bar{t}$ production [26]. At the same time we find that the significance of the resulting signal does depend on the assumptions made on the cuts needed against reducible backgrounds (mainly from QCD and detector misidentifications).

[6] A calculation with all available corrections is not possible here because the phases lead to numerical instabilities.

In the standard maximal mixing scenario of the MSSM, using the softer cuts ($p_{\perp\tau_{\text{jet}}} > 50$ GeV and $\not{p}_\perp > 50$ GeV) we find a viable signal in the case of large $\tan\beta$ ($\gtrsim 30$) and intermediate charged Higgs masses ($150\,\text{GeV} \lesssim m_{H^\pm} \lesssim 300\,\text{GeV}$), whereas with the harder cuts ($p_{\perp\tau_{\text{jet}}} > 100$ GeV and $\not{p}_\perp > 100$ GeV) we only find a viable signal for $\tan\beta \gtrsim 50$ if in addition an appropriate upper cut on $m_\perp = \sqrt{2p_{\perp\tau_{\text{jet}}}\not{p}_\perp[1-\cos(\Delta\phi)]}$ is applied. Thus, in the best case the associated charged Higgs and W boson production could serve as a complement to production in association with top quarks in the difficult transition region $m_{H^\pm} \sim m_t$ although only for large $\tan\beta$, but before one can draw any firm conclusions the effects of reducible backgrounds have to be studied in more detail.

In MSSM scenarios with less or no mixing in the third generation squark sector we get similar results as in the standard maximal mixing scenario. In fact, the differences compared to the maximal mixing scenario are in both cases smaller than the $\mathcal{O}$ (10%–20%) effects we expect from higher order electroweak and QCD corrections as well as other variations of the SUSY scenario. Similarly we have also found that the cross-section depends only weakly on the CP-violating phases of the SUSY parameters, even those of A_t and μ, which result in a mixing between the CP-even and CP-odd Higgs bosons. This is a general feature that will be true as long as the differences in the neutral Higgs bosons masses are small compared to the charged Higgs plus W boson mass (more specifically $m^2_{H_i} - m^2_{H_j} \ll (m_{H^\pm} + m_W)^2 - m^2_{H_i}$) even if the Higgs mixing matrix is highly non-diagonal. The phases of A_t and μ also lead to differences in the masses of the neutral Higgs bosons. In fact, we have seen that the main effect on the cross-section comes from these kinematic effects of the Higgs masses and not from the changes in the couplings due to the phases.

We have also studied a class of special resonant scenarios where $m_{H_i} \gtrsim m_{H^\pm} + m_W$ for one of the neutral Higgs bosons (the CP-odd Higgs A in the MSSM with real parameters) leading to resonant production in the s-channel. This results in a very large enhancement of the total cross-section (up to a factor 100) in the region of intermediate $\tan\beta$ (~ 10). However, due to the different kinematics of resonant production, the significance of the signal depends very strongly on the $p_{\perp\tau_{\text{jet}}}$ and $\not{p}_\perp$ cuts. With the softer cuts we get a significance of order 50 in the case of $m_{H^\pm} = 175$ GeV, whereas with the harder ones it drops to 0.2. Another problem with this type of MSSM scenarios is that for larger charged Higgs masses ($m_{H^\pm} \gtrsim 200$ GeV) the possibility of decays to squarks opens up, which would require a different type of analysis.

One may also worry about the perturbative stability of these resonant scenarios with very large one-loop corrections to the mass of the CP-odd Higgs boson. However, comparing the one-loop and available two-loop corrections, as was done in Table 5, this does not seem to be the case. When making a sparse scan of parameters we find similar scenarios in a large range of $\tan\beta$ and $m_{H^\pm}$, and we also get similar results when using CPSUPERH instead of FEYNHIGGS although not precisely at the same points

in parameter space. We have also found that in these resonant scenarios the cross-section can have a large dependence on the CP-violating phases of the SUSY parameters, but we have not found any appreciable CP-asymmetries. However, we have not been able to make a more thorough study of the sensitivity to these phases, which would require a separate study.

Finally, it should be emphasized that our study is specifically for different MSSM scenarios and that the conclusions may change in other models. For example, in a general 2HDM, the resonant enhancement is more natural since the Higgs masses are independent of each other. In addition, there will be no charged Higgs decays to squarks as we found in the MSSM, thus making it possible to have a clear signal for large charged Higgs masses even with the harder cuts against reducible backgrounds. Similarly non-minimal supersymmetric models with larger Higgs sectors may also offer more natural possibilities for resonant enhancement.

Acknowledgements. We would like to thank Gunnar Ingelman for comments on the manuscript. This work has been supported by the Göran Gustafsson Foundation. S.H. is supported by the German Federal Ministry of Education and Research (BMBF) under contract number 05HT4WWA/2. J.R. is supported by the Swedish Research Council, contract number 629-2001-5873.

References

1. LEP Higgs Working Group for Higgs boson searches, hep-ex/0107031
2. Particle Data Group, S. Eidelman et al., Phys. Lett. B **592**, 1 (2004)
3. R.M. Barnett, H.E. Haber, D.E. Soper, Nucl. Phys. B **306**, 697 (1988)
4. A.C. Bawa, C.S. Kim, A.D. Martin, Z. Phys. C **47**, 75 (1990)
5. F. Borzumati, J.-L. Kneur, N. Polonsky, Phys. Rev. D **60**, 115 011 (1999) [hep-ph/9905443]
6. D.J. Miller, S. Moretti, D.P. Roy, W.J. Stirling, Phys. Rev. D **61**, 055 011 (2000) [hep-ph/9906230]
7. J.F. Gunion, Phys. Lett. B **322**, 125 (1994) [hep-ph/9312201]
8. V.D. Barger, R.J.N. Phillips, D.P. Roy, Phys. Lett. B **324**, 236 (1994) [hep-ph/9311372]
9. S. Raychaudhuri, D.P. Roy, Phys. Rev. D **53**, 4902 (1996) [hep-ph/9507388]
10. S. Moretti, K. Odagiri, Phys. Rev. D **55**, 5627 (1997) [hep-ph/9611374]
11. D.P. Roy, Phys. Lett. B **459**, 607 (1999) [hep-ph/9905542]
12. S. Moretti, D.P. Roy, Phys. Lett. B **470**, 209 (1999) [hep-ph/9909435]
13. A. Belyaev, D. Garcia, J. Guasch, J. Sola, JHEP **06**, 059 (2002) [hep-ph/0203031]
14. C. Biscarat, M. Dosil, Charged Higgs search in top quark decays with the ATLAS detector, ATL-PHYS-2003-038, 2003.
15. K.A. Assamagan, Y. Coadou, Acta Phys. Pol. B **33**, 707 (2002)
16. R. Kinnunen, Study of Heavy Charged Higgs in $pp \to tH^{\pm}$ with $H^{\pm} \to \tau\nu$ in CMS, CMS NOTE 2000/045 (available from http://cmsdoc.cern.ch/doc/notes/docs/NOTE2000_045), 2000
17. M. Bisset, M. Guchait, S. Moretti, Eur. Phys. J. C **19**, 143 (2001) [hep-ph/0010253]
18. M. Bisset, F. Moortgat, S. Moretti, Eur. Phys. J. C **30**, 419 (2003) [hep-ph/0303093]
19. C. Hansen, N. Gollub, K. Assamagan, T. Ekelof, Eur. Phys. J. C **44S2**, 1 (2005) [hep-ph/0504216]
20. M. Guchait, S. Moretti, JHEP **01**, 001 (2002) [hep-ph/0110020]
21. K.A. Assamagan, M. Guchait, S. Moretti, hep-ph/0402057 (2004)
22. J. Alwall, J. Rathsman, JHEP **12**, 050 (2004) [hep-ph/0409094]
23. B. Mohn, M. Flechl, J. Alwall, ATLAS discovery potential for the Charged Higgs Boson in $H^{+} \to \tau\nu$ decays, ATL-PHYS-PUB-2007-006, 2007
24. D.A. Dicus, J.L. Hewett, C. Kao, T.G. Rizzo, Phys. Rev. D **40**, 787 (1989)
25. A.A. Barrientos Bendezu, B.A. Kniehl, Phys. Rev. D **59**, 015 009 (1999) [hep-ph/9807480]
26. S. Moretti, K. Odagiri, Phys. Rev. D **59**, 055 008 (1999) [hep-ph/9809244]
27. A.A. Barrientos Bendezu, B.A. Kniehl, Phys. Rev. D **61**, 097 701 (2000) [hep-ph/9909502]
28. A.A. Barrientos Bendezu, B.A. Kniehl, Phys. Rev. D **63**, 015 009 (2001) [hep-ph/0007336]
29. O. Brein, W. Hollik, S. Kanemura, Phys. Rev. D **63**, 095 001 (2001) [hep-ph/0008308]
30. Y.-S. Yang, C.-S. Li, L.-G. Jin, S.H. Zhu, Phys. Rev. D **62**, 095 012 (2000) [hep-ph/0004248]
31. W. Hollik, S.-H. Zhu, Phys. Rev. D **65**, 075 015 (2002) [hep-ph/0109103]
32. J. Zhao, C.S. Li, Q. Li, Phys. Rev. D **72**, 114 008 (2005) [hep-ph/0509369]
33. E. Asakawa, O. Brein, S. Kanemura, Phys. Rev. D **72**, 055 017 (2005) [hep-ph/0506249]
34. Q.-H. Cao, S. Kanemura, C.P. Yuan, Phys. Rev. D **69**, 075 008 (2004) [hep-ph/0311083]
35. H. Eberl, K. Hidaka, S. Kraml, W. Majerotto, Y. Yamada, Phys. Rev. D **62**, 055 006 (2000) [hep-ph/9912463]
36. M. Carena, D. Garcia, U. Nierste, C.E.M. Wagner, Nucl. Phys. B **577**, 88 (2000) [hep-ph/9912516]
37. M. Carena, S. Heinemeyer, C.E.M. Wagner, G. Weiglein, hep-ph/0511023 (2005)
38. A. Pilaftsis, Phys. Lett. B **435**, 88 (1998) [hep-ph/9805373]
39. A. Pilaftsis, C.E.M. Wagner, Nucl. Phys. B **553**, 3 (1999) [hep-ph/9902371]
40. A.G. Akeroyd, S. Baek, Phys. Lett. B **500**, 142 (2001) [hep-ph/0008286]
41. J.R. Ellis, J.S. Lee, A. Pilaftsis, Phys. Rev. D **70**, 075 010 (2004) [hep-ph/0404167]
42. A. Pilaftsis, Nucl. Phys. B **504**, 61 (1997) [hep-ph/9702393]
43. E. Christova, H. Eberl, W. Majerotto, S. Kraml, Nucl. Phys. B **639**, 263 (2002) [hep-ph/0205227]
44. J.A. Williams, hep-ph/0505121 (2005)
45. M. Carena, J.R. Ellis, A. Pilaftsis, C.E.M. Wagner, Nucl. Phys. B **586**, 92 (2000) [hep-ph/0003180]
46. J.S. Lee et al., Comput. Phys. Commun. **156**, 283 (2004) [hep-ph/0307377]

47. S. Heinemeyer, Eur. Phys. J. C **22**, 521 (2001) [hep-ph/0108059]
48. T. Hahn, W. Hollik, S. Heinemeyer, G. Weiglein, (2005) [hep-ph/0507009]
49. T. Hahn, W. Hollik, S. Heinemeyer, G. Weiglein, FeynHiggs version 2.2.10, http://www.feynhiggs.de
50. M. Frank et al., hep-ph/0611326 (2006)
51. D. Eriksson, http://www.isv.uu.se/thep/MC/pybbwh/
52. T. Sjöstrand et al., Comput. Phys. Commun. **135**, 238 (2001) [hep-ph/0010017]
53. T. Sjöstrand, L. Lönnblad, S. Mrenna, P. Skands, hep-ph/0308153 (2003)
54. CTEQ, H.L. Lai et al., Eur. Phys. J. C **12**, 375 (2000) [hep-ph/9903282]
55. W.K. Tung et al., JHEP **02**, 053 (2007) [hep-ph/0611254]
56. M.L. Mangano, M. Moretti, F. Piccinini, R. Pittau, A.D. Polosa, JHEP **07**, 001 (2003) [hep-ph/0206293]
57. H. Murayama, I. Watanabe, K. Hagiwara, KEK-91-11
58. T. Stelzer, W.F. Long, Comput. Phys. Commun. **81**, 357 (1994) [hep-ph/9401258]
59. F. Maltoni, T. Stelzer, JHEP **02**, 027 (2003) [hep-ph/0208156]
60. S. Jadach, J.H. Kühn, Z. Was, Comput. Phys. Commun. **64**, 275 (1990)
61. P. Golonka et al., hep-ph/0312240 (2003)
62. D.P. Roy, Phys. Lett. B **277**, 183 (1992)
63. M. Guchait, R. Kinnunen, D.P. Roy, hep-ph/0608324 (2006)
64. R. Brenner, private communication
65. M. Carena, S. Heinemeyer, C.E.M. Wagner, G. Weiglein, Eur. Phys. J. C **26**, 601 (2003) [hep-ph/0202167]
66. Muon g-2, G.W. Bennett et al., Phys. Rev. Lett. **92**, 161 802 (2004) [hep-ex/0401008]
67. M. Davier, W.J. Marciano, Ann. Rev. Nucl. Part. Sci. **54**, 115 (2004)
68. B.C. Regan, E.D. Commins, C.J. Schmidt, D. DeMille, Phys. Rev. Lett. **88**, 071 805 (2002)
69. P.G. Harris et al., Phys. Rev. Lett. **82**, 904 (1999)
70. M.V. Romalis, W.C. Griffith, E.N. Fortson, Phys. Rev. Lett. **86**, 2505 (2001) [hep-ex/0012001]
71. T. Ibrahim, P. Nath, Phys. Rev. D **58**, 111 301 (1998) [hep-ph/9807501]
72. T. Ibrahim, P. Nath, Phys. Rev. D **61**, 093 004 (2000) [hep-ph/9910553]
73. A. Bartl, T. Gajdosik, W. Porod, P. Stockinger, H. Stremnitzer, Phys. Rev. D **60**, 073 003 (1999) [hep-ph/9903402]
74. V.D. Barger et al., Phys. Rev. D **64**, 056 007 (2001) [hep-ph/0101106]
75. S. Abel, S. Khalil, O. Lebedev, Nucl. Phys. B **606**, 151 (2001) [hep-ph/0103320]
76. S.Y. Choi, M. Drees, B. Gaissmaier, Phys. Rev. D **70**, 014 010 (2004) [hep-ph/0403054]
77. M. Pospelov, A. Ritz, Ann. Phys. **318**, 119 (2005) [hep-ph/0504231]
78. K.A. Olive, M. Pospelov, A. Ritz, Y. Santoso, Phys. Rev. D **72**, 075 001 (2005) [hep-ph/0506106]
79. S. Abel, O. Lebedev, JHEP **01**, 133 (2006) [hep-ph/0508135]
80. S. Yaser Ayazi, Y. Farzan, hep-ph/0605272 (2006)
81. A. Bartl, W. Majerotto, W. Porod, D. Wyler, Phys. Rev. D **68**, 053 005 (2003) [hep-ph/0306050]
82. A.G. Akeroyd, S. Baek, Phys. Lett. B **525**, 315 (2002) [hep-ph/0105228]
83. B. Mohn, N. Gollub, K.A. Assamagan, Study of the $H^{\pm} \to W^{\pm}H^0$ decay in a large mass splitting MSSM scenario with ATLAS, ATL-PHYS-PUB-2005-017